JLR RESEARCH ARTICLE

Simvastatin inhibits POVPC-mediated induction of endothelial-to-mesenchymal cell transition

Yan Li[1,2,3,4,‡], Yi-Xin Zhang[1,2,3,4,‡], Da-Sheng Ning[1,2,3,4,‡], Jing Chen[2,3,4,5,‡], Shang-Xuan Li[1,2,3,4,‡], Zhi-Wei Mo[1,2,3,4], Yue-Ming Peng[1,2,3,4], Shi-Hui He[1,2,3,4], Ya-Ting Chen[1,2,3,4], Chun-Juan Zheng[1,2,3,4], Jian-Jun Gao[1,2,3,4], Hao-Xiang Yuan[1,2,3,4], Jing-Song Ou[1,2,3,4,6,*], and Zhi-Jun Ou[2,3,4,5,*]

[1]Division of Cardiac Surgery, Heart Center, The First Affiliated Hospital, Sun Yat-sen University, Guangzhou, People's Republic of China; [2]National-Guangdong Joint Engineering Laboratory for Diagnosis and Treatment of Vascular Diseases, Guangzhou, People's Republic of China; [3]NHC key Laboratory of Assisted Circulation (Sun Yat-sen University), Guangzhou, People's Republic of China; [4]Guangdong Provincial Engineering and Technology Center for Diagnosis and Treatment of Vascular Diseases, Guangzhou, People's Republic of China; [5]Division of Hypertension and Vascular Diseases, Department of Cardiology, Heart Center, The First Affiliated Hospital, Sun Yat-sen University, Guangzhou, People's Republic of China; and [6]Guangdong Provincial Key Laboratory of Brain Function and Disease, Zhongshan School of Medicine, Sun Yat-sen University, Guangzhou, People's Republic of China

Abstract Endothelial-to-mesenchymal transition (EndMT), the process by which an endothelial cell (EC) undergoes a series of molecular events that result in a mesenchymal cell phenotype, plays an important role in atherosclerosis. 1-Palmitoyl-2-(5-oxovaleroyl)-sn-glycero-3-phosphocholine (POVPC), derived from the oxidation of 1-palmitoyl-2-arachidonoyl-sn-glycero-3-phosphatidylcholine, is a proinflammatory lipid found in atherosclerotic lesions. Whether POVPC promotes EndMT and how simvastatin influences POVPC-mediated EndMT remains unclear. Here, we treated human umbilical vein ECs with POVPC, simvastatin, or both, and determined their effect on EC viability, morphology, tube formation, proliferation, and generation of NO and superoxide anion ($O_2^{\cdot-}$). Expression of specific endothelial and mesenchymal markers was detected by immunofluorescence and immunoblotting. POVPC did not affect EC viability but altered cellular morphology from cobblestone-like ECs to a spindle-like mesenchymal cell morphology. POVPC increased O_2^{-} generation and expression of alpha-smooth muscle actin, vimentin, Snail-1, Twist-1, transforming growth factor-beta (TGF-β), TGF-β receptor II, p-Smad2/3, and Smad2/3. POVPC also decreased NO production and expression of CD31 and endothelial NO synthase. Simvastatin inhibited POVPC-mediated effects on cellular morphology, production of $O_2^{\cdot-}$ and NO, and expression of specific endothelial and mesenchymal markers. These data demonstrate that POVPC induces EndMT by increasing oxidative stress, which stimulates TGF-β/Smad signaling, leading to Snail-1 and Twist-1 activation. Simvastatin inhibited POVPC-induced EndMT by decreasing oxidative stress, suppressing TGF-β/Smad signaling, and inactivating Snail-1 and Twist-1. Our findings reveal a novel mechanism of atherosclerosis that can be inhibited by simvastatin.

Supplementary key words atherosclerosis • CVD • cell biology • endothelial cells • LDL • NO • oxidized lipids • signal transduction • superoxide anion • vascular biology

Atherosclerosis is a chronic inflammatory and multifactorial disease (1, 2). However, its mechanisms remain unclear. Endothelial dysfunction is a marker of atherosclerotic risk and an early predictor of atherosclerosis development (3). Recent studies have demonstrated that endothelial-to-mesenchymal transition (EndMT) may contribute to the occurrence of CVDs, including atherosclerosis, pulmonary hypertension, cardiac fibrosis, Kawasaki disease, as well as diabetes (4–8). In the pathobiology of atherosclerosis, EndMT has been found to contribute to the fibrotic process of atherosclerotic plaque formation and plaque instability (9, 10). Endothelial cells (ECs) acquire a fibroproliferative mesenchymal phenotype through EndMT (11, 12). Thus, EndMT plays an important role in the development of atherosclerosis (6).

Previous studies have reported several proinflammatory lipids in atherosclerotic plaques (13, 14), of which 1-palmitoyl-2-(5-oxovaleroyl)-sn-glycero-3-phos phocholine (POVPC) is a major one (15–18). Further studies have shown that POVPC modulates several major cell types involved in atherosclerosis, including monocytes, ECs, vascular smooth muscle cells, and lymphocytes (13, 17, 19, 20). POVPC is a powerful endothelial activator (21). Yeh *et al.* (22) found that POVPC upregulates the expression of inflammatory factors, including

‡These authors contributed equally to this work.
*For correspondence: Jing-Song Ou, oujs2000@163.com, oujs2000@yahoo.com; Zhi-Jun Ou, Zhijunou@163.com.

 https://doi.org/10.1016/j.jlr.2021.100066

fibronectin, monocyte chemoattractant protein-1, and interleukin-8 in ECs. Recently, we demonstrated that POVPC impairs endothelial function (23). However, whether POVPC induces EndMT remains unclear.

Statins have been widely used for the inhibition of atherosclerosis as they reduce cholesterol and blood lipids and especially inhibit oxidized LDL (oxLDL)-induced atherosclerosis (24, 25). Whether statins inhibit atherosclerosis by limiting EndMT remains unknown. Moreover, oxLDL has been found to induce EndMT (26, 27). POVPC is derived from oxidation of 1-palmitoyl-2-arachidonoyl-sn-glycero-3-phosphatidylcholine (PAPC), one of many oxidized lipid species present in oxLDL. Simvastatin is a statin used to inhibit atherosclerosis, including oxLDL-induced atherosclerosis (24). However, it is unclear whether oxLDL induces EndMT through POVPC. It is also unclear whether simvastatin inhibits oxLDL-induced atherosclerosis by reducing POVPC-induced EndMT. Therefore, in the present study, we sought to investigate POVPC-mediated EndMT induction and the effect of simvastatin on POVPC-mediated EndMT.

MATERIALS AND METHODS

Cell culture

Human umbilical vein endothelial cells (HUVECs) were obtained from ScienCell (Carlsbad, CA). Cells between passages 4–6 were used in all experiments. The cells were grown in endothelial cell medium containing 5% FBS, 1% EC growth factor supplement, and 1% antibiotic (ScienCell) and maintained at 37°C in a humidified atmosphere of 95% air and 5% CO_2. Cells were harvested at the time points indicated. Cells were plated in 6-, 48-, or 96-well plates, grown until confluent, and synchronized by maintaining them in 0.5% serum overnight before treatment. To study the effects of POVPC (Avanti Polar Lipids Inc, Alabaster, AL) on EndMT, the cells were treated with POVPC or simvastatin for at least 48 h providing the ECs sufficient time to transform to mesenchymal cells.

Cell viability assay

The cytotoxic effects of POVPC in HUVECs were examined using the Cell Counting Kit-(CCK-8) assay. Briefly, HUVECs (2×10^4 cells/well) were plated in 96-well plates and treated with POVPC (25 μM) for 12, 24, and 48 h. CCK-8 solution (10 μl, Dojindo, Shanghai, China) was then added to each well and incubated for 4 h at 37°C. The absorbance was measured at 450 nm using a microplate reader (Thermo, Waltham, MA). The percentage of living cells in the treated cultures was calculated relative to that in the untreated cultures.

Tube formation assay

EC tube formation was assessed using the basement membrane matrix gel to determine whether POVPC attenuates angiogenesis in HUVECs, as described previously (23, 28). Briefly, Matrigel was added to each well of 96-well culture plates and incubated at 37°C for 1 h. HUVECs (2×10^5 cells/ml) were added to the Matrigel-coated 96-well plates and cultured for 12 h. The cells were then treated with POVPC (25 μM) with or without simvastatin (0.1 μM; Sigma-Aldrich, St. Louis, MO) and incubated at 37°C for 6 h. EC tube formation was photographed using a microscope. The data were analyzed using ImageJ software (National Institutes of Health).

5-Ethynyl-20-deoxyuridine assay

5-Ethynyl-20-deoxyuridine (EdU) assay was performed using an EdU labeling detection kit (EdU; RiboBio Co, Ltd, Guangzhou, China). HUVECs were treated with POVPC (25 μM), simvastatin (0.1 μM), or both for 48 h. The cells were then incubated with 50 μmol/l EdU for 6 h and fixed in 4% paraformaldehyde for 30 min at about 25°C. The HUVECs were treated with 2 mg/ml glycine for 5 min. After washing with PBS, 200 μl of 0.5% Triton X-100 was added to each well and incubated for 10 min. The wells were washed twice with PBS and stained with 100 μl of 1xApollo® reaction cocktail for 30 min at about 25°C. Subsequently, the DNA in the HUVECs was stained with Hoechst 33342 for 30 min. Images were obtained using a fluorescence microscope (DMi8; Leica, Wetzlar, Germany). The EdU-positive cell index was calculated as a ratio of the number of positive cells to the total number of cells.

Quantitative real-time RT-PCR

The expression levels of various genes were analyzed using quantitative RT-PCR (qRT-PCR). Total RNA was extracted using TRIzol reagent (Sigma-Aldrich) according to the manufacturer's instructions. cDNA was synthesized using the Transcriptor® First Strand cDNA Synthesis Kit (Roche, Mannheim, Germany). RT-PCR was carried out using a LightCycler® 480 SYBR Green I Master (Roche). Primer sequences used were as follows: *CD31*, forward, 5'-CCACGCCTAGC CAAAATCAC-3' and reverse, 5'-CATGTGGCCCCTCAGAA GAC-3'. Vascular endothelial *(VE)-cadherin*, forward, 5'-ATGA-GATCGTGGTGGAAGCG-3' and reverse, 5'-ATGTG TACTTGGTCTGGGTGA-3'. Alpha-smooth muscle actin (*α-SMA*), forward, 5'-AAGCACAGAGAGCAAAAGAGG AAT-3' and reverse, 5'-ATGTCGTCCCAGTTGGTGAT-3'. *VIM* (*Vimentin*), forward, 5'-TCCGCACATTCGAGCAAAGA-3' and reverse, 5'-TGAGGGCTCCTAGCGGTTTA-3'. *eNOS*, forward 5'-AGCACATTTGGGAATGGGGAT-3' and reverse, 5'-AGAGGACACCAGTGGGTCTG-3'. *SMAD2*, forward, 5'-GGAG CAGAATACCGAAGGCA-3' and reverse, 5'-CTTGAGCAA CGCACTGAAGG-3'. *SMAD3*, forward, 5'-ATTCCAGAAAC GCCACCTCC-3' and reverse, 5'-GCTATTGAACACCAAAA TGCAGG-3'. *ACTB* (*β-actin*), forward, 5'-GCCATGTACGTAGC CATCCA-3' and reverse, 5'-GAACCGCTCATTGCCGATAG-3'. All samples were analyzed using a Bio-Rad real-time analyzer.

Measurement of NO generation

HUVECs were cultured to 90% confluence. The cells were serum starved with 0.5% FBS and pretreated with POVPC (25 μM) with and without simvastatin (0.1 μM) or vascular endothelial growth factor (VEGF; 50 ng/ml; R&D Systems, Minneapolis, MN) for 12 h. N^G-monomethyl-L-arginine (1 mM, Millipore Corp, Billerica, MA) was then added into half of the cultured plates and incubated for 36 h. The HUVECs were then incubated with 4,5-diaminofluoresce in diacetate (10 μM; Merck, Darmstadt, Germany) containing L-arginine (25 μM; Sigma-Aldrich) and A23187 (5 μM; Calbiochem, Merck) for 30 min at

37°C. Fluorescence was monitored using fluorescence microscopy. The relative change was analyzed using the ImageJ analysis software, as described previously (29–31). In addition, the supernatant from each well was used to detect the generation of NO using a Sievers NOA analyzer (GE Analytical Instruments, Boulder, CO) as described previously (32, 33).

RNA interference

SiRNA gene expression knockdown studies were performed using Lipofectamine® RNAiMAX and the corresponding manufacturer's protocol. siRNA (10 nmol each) was transfected into cells using Lipofectamine® RNA iMAX transfection reagent (Invitrogen, Carlsbad, CA) following the manufacturer's guidelines. Snail-1 siRNA sequences were synthesized according to the method of Medici *et al.* (34). siRNA was synthesized by Guangzhou RiboBio Co, Ltd.

Measurement of superoxide anion ($O_2^{\bullet -}$) generation

HUVECs were cultured to 90% confluence. They were serum starved with 0.5% FBS and pretreated with POVPC (25 μM) with and without simvastatin (0.1 μM; Sigma-Aldrich) and TNF-α (10 μM; Sigma-Aldrich) as a positive control for 12 h. N(ω)-nitro-L-arginine methyl ester (L-NAME; 1 mM; Sigma-Aldrich), manganese-5, 10, 15, 20-tetrakis (4-benzoic acid) porphyrin (Mn-TBAP, 10 mM; Cayman, Ann Arbor, MI), *N*-acetylcysteine (NAC; 1 mM; Sigma-Aldrich), diphenyleneiodonium (DPI; 10 μM; Sigma-Aldrich), or rotenone (2 μM; Sigma-Aldrich) as the scavenger of oxygen free radicals were added to half of the cultured plates and incubated for 36 h. Then, the cells were washed twice with HBSS and incubated with 10 μM dihydroethidium (DHE; Sigma-Aldrich) containing L-arginine (25 μM) and A23187 (5 μM) for 30 min at 37°C. Fluorescence images were obtained using fluorescence microscopy, and the relative change was analyzed using the ImageJ analysis software, as previously described (29–31).

Immunofluorescence staining

HUVECs were cultured to 90% confluence, serum starved with 0.5% FBS, and treated with POVPC (25 μM) with and without simvastatin (0.1 μM) for 48 h. They were fixed in 4% paraformaldehyde at about 25°C for 30 min and then washed with PBS. Nonspecific immunoreactions were blocked using 5% BSA + 0.1% Triton X + 0.1% Tween 20 in PBS for 1 h at about 25°C. Cells were washed in PBS and incubated with a primary antibody against CD31 (1:1,000; Abcam, Cambridge, MA), VE-cadherin (1:500; Cell Signaling Technology, Danvers, MA), vimentin (1:500; Cell Signaling Technology), α-SMA (1:100; Abcam), eNOS (1:200; Santa Cruz, Dallas, TX), Smad2/3 (1:200; Cell Signaling Technology), Snail-1 (1:200; Santa Cruz), and Twist-1 (1:200; Sigma-Aldrich) overnight at 4°C. Following washing, the cells were incubated in goat anti-mouse IgG secondary antibody conjugated to Alexa Fluor 555 (1:1,000; Cell Signaling Technology) and goat anti-rabbit IgG secondary antibody conjugated to Alexa Fluor 488 (1:1,000; Cell Signaling Technology) overnight at 4°C. F-actin was stained with phalloidin (1:1,000; Cell Signaling Technology). Cells were then washed with PBS and counter stained with Hoechst 33342 (1 μg/ml; Cell Signaling Technology) for 5 min. Images were obtained using a laser-scanning confocal microscope (LSM780; Carl Zeiss, Jena, Germany).

Western blot analysis

HUVECs were cultured in endothelial cell medium supplemented with 5% FBS, 1% growth factors, and 1% penicillin/streptomycin. The cells were treated with POVPC (25 μM) with and without simvastatin (0.1 μM) for 48 h. The cells were then washed three times with PBS and lysed in RIPA buffer (Cell Signaling Technology). Proteins were separated using SDS-PAGE and transferred to PVDF membranes. The membranes were blocked with 5% BSA in TBS with 0.1% Tween® 20 detergent for 2 h at about 25°C. The primary antibodies against VE-cadherin (Cell Signaling Technology), α-SMA (Abcam), CD31 (Cell Signaling Technology), vimentin (Cell Signaling Technology), phospho-Smad2/3 (Cell Signaling Technology), Smad2/3 (Cell Signaling Technology), transforming growth factor-beta (TGF-β; Cell Signaling Technology), TGF-β receptor II (Bioss, Boston, MA), eNOS (Santa Cruz), Snail-1 (Santa Cruz), and β-actin (Cell Signaling Technology) were used for detecting the proteins by overnight incubation at 4°C. The membranes were washed three times with TBS with 0.1% Tween® 20 detergent and incubated with a horseradish peroxidase-coupled secondary antibody for 1 h at about 25°C. The protein bands were detected using a chemiluminescence detection kit (Millipore Corp). Blots were quantified using ImageJ software.

Statistical analysis

Statistical analyses were performed using SPSS 21.0 software (SPSS, Chicago, IL). Significant differences in mean values were determined using one-way ANOVA followed by a Tukey test for more than two groups or with Student's *t*-test for two groups. P values <0.05 were considered statistically significant. Data are expressed as mean ± SEM.

RESULTS

Effects of POVPC in the morphology and cell viability of ECs

As shown in supplemental Fig. S1, treatment of HUVECs with 25 μM POVPC for 48 h caused a substantial change in their cellular morphology from an endothelial cobblestone-like form to an elongated spindle-shaped form, characteristic of EndMT. HUVECs incubated with 12.5 μM POVPC exhibited a nontypical elongated spindle shape, whereas those incubated with 50 μM of POVPC exhibited a large number of dead cells (supplemental Fig. S1). As shown in **Fig. 1**A, treatment of HUVECs with POVPC (25 μM) for 12 h caused a substantial change in cellular morphology from the endothelial cobblestone-like form to an elongated spindle-shaped form after 48 h. CCK-8 assay was used to determine if POVPC impaired HUVEC proliferation after 12, 24, and 48 h of treatment. We found that the EC numbers did not change after treatment with POVPC when compared with the controls (Fig. 1B).

POVPC induces HUVECs to undergo EndMT

To further analyze the POVPC-induced changes in cellular morphology, EndMT markers were detected using qRT-PCR, immunofluorescence, and Western blotting. qRT-PCR analysis showed that POVPC decreased the expression of *CD31* mRNAs but increased *α-SMA* and *VIM (vimentin)* mRNA levels. mRNA expression of *CD31* showed a time-dependent

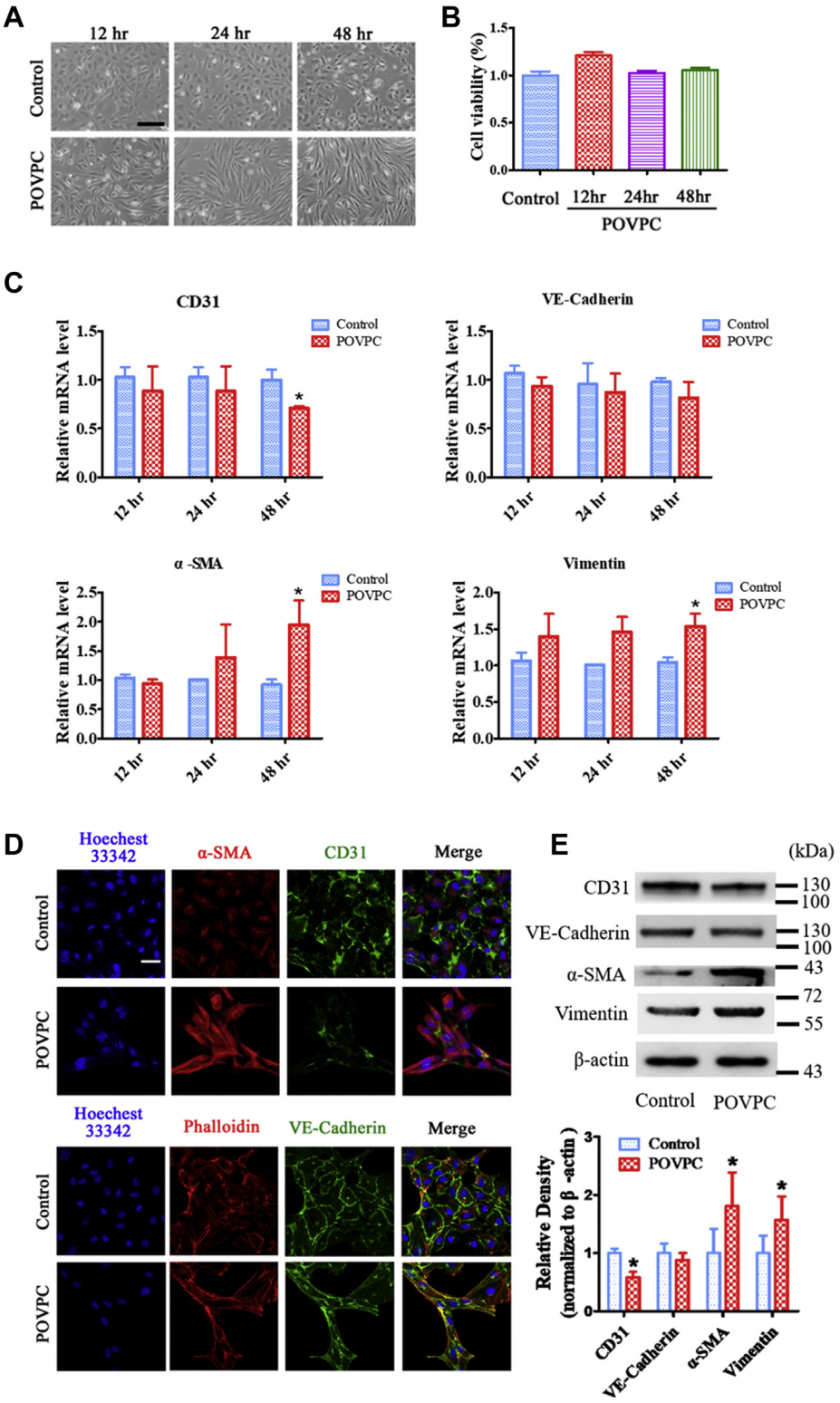

Fig. 1. POVPC induces EndMT in cultured HUVECs. A: Representative light microscopic images showing cells with typical cobblestone morphology in control versus cells with a fibroblast-like phenotype in cultured HUVECs following exposure to POVPC for 12, 24, and 48 h. B: POVPC did not inhibit HUVEC survival rate. C: qRT-PCR showing the intracellular mRNA levels of *CD31*, *VE-cadherin*, *α-SMA*, and *VIM* (*vimentin*) after pretreated with POVPC for 12, 24, and 48 h in cultured HUVECs. D: Immunofluorescence microscopy shows a decrease in the fluorescent intensity of CD31 (green) and an increase in fluorescent intensity of α-SMA (red) after treatment of cultured HUVECs with POVPC for 48 h. There was no significant change in the fluorescent intensity of VE-cadherin (green). F-actin was stained with phalloidin (red). Nuclei were stained with Hoechst 33342 (blue). E: Western blots and bar charts showing the protein levels of CD31, VE-cadherin, α-SMA, and vimentin after pretreatment of cultured HUVECs with POVPC for 48 h (*vs. corresponding control group; $P < 0.05$, $n = 8$). The scale bars represent 100 μm in A and 30 μm in D.

decrease, whereas those of *α-SMA* and *VIM (vimentin)* showed a time-dependent increase (Fig. 1C). Immunofluorescence staining showed that the expression of CD31 in ECs was significantly inhibited after pretreatment with POVPC for 48 h, and the expression of α-SMA was increased in the POVPC group compared with that in the control group (Fig. 1D). However, the expression of VE-cadherin was not significantly different between the POVPC and control groups (Fig. 1D). In addition, Western blotting results showed that POVPC upregulated the expression of α-SMA and vimentin and downregulated the expression of the EC marker, CD31, compared with the control (Fig. 1E). In addition, TGF-β (5 μg/ml) and interleukin-1β (10 ng/ml) were used as positive controls in parallel for comparison of the POVPC-induced EndMT. The data showed that POVPC-induced EndMT differed in both rate and degree compared with that induced by the positive controls (supplemental Fig. S2).

Simvastatin treatment suppresses POVPC-induced EndMT and conserves the endothelial phenotype

The effect of simvastatin on POVPC-mediated EndMT was examined in cultured ECs. Simvastatin itself did not affect the endothelial phenotype (**Fig. 2**A). HUVECs were treated with POVPC and simvastatin for 48 h. The cells presented as typical rounded or cobblestone shapes, suggesting that simvastatin inhibited POVPC-induced transformation of the cell shape from cobblestone-like to spindle-like (Fig. 2A) form. Furthermore, simvastatin decreased the expression of α-SMA and vimentin and increased the expression of CD31 induced by POVPC (Fig. 2A–D).

Effects of POVPC and simvastatin on EC tube formation

To test whether simvastatin affects POVPC-impaired endothelial function during EndMT, the effects of POVPC and simvastatin on EC tube formation were investigated. POVPC impaired EC tube formation, whereas simvastatin inhibited the POVPC-impaired EC tube formation (**Fig. 3**A, B).

Effects of POVPC and simvastatin on EC proliferation

Next, the effect of POVPC on EC proliferation was examined using the EdU assay in EndMT. POVPC inhibited EC proliferation, whereas simvastatin significantly restored the proliferation of ECs inhibited by POVPC (Fig. 3C, D).

Effects of POVPC and simvastatin on $O_2^{\bullet-}$ generation in ECs

To further investigate the mechanisms of POVPC-induced EndMT, the effects of POVPC on $O_2^{\bullet-}$

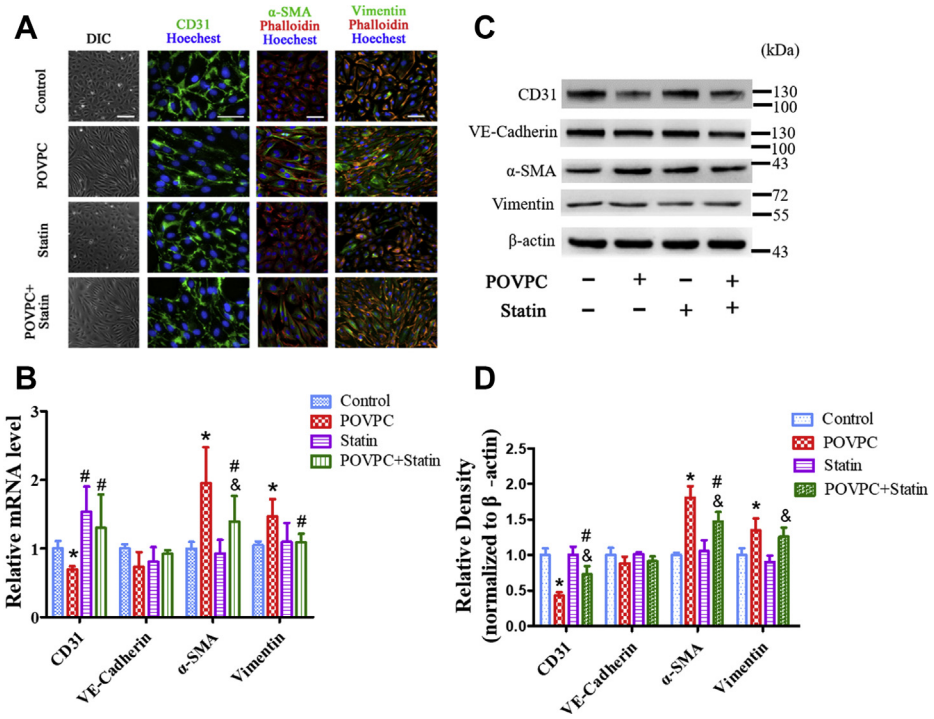

Fig. 2. Simvastatin inhibited POVPC-induced EndMT in cultured HUVECs. A: HUVECs were analyzed by immunofluorescence for the expression of CD31 (green), α-SMA (green), and vimentin (green) after pretreatment with POVPC with or without simvastatin. F-actin was stained with phalloidin (red). The nuclei were stained with Hoechst 33342 (blue). B: qRT-PCR showing the intracellular mRNA levels of *CD31*, *VE-cadherin*, *α-SMA*, and *VIM (vimentin)* after pretreated with POVPC and/or simvastatin for 48 h in cultured HUVECs. C and D: The relative protein levels of CD31, VE-cadherin, α-SMA, and vimentin cultured HUVECs were assessed using Western blotting (* vs. corresponding control group; #vs. POVPC group, & vs. statin group; $P < 0.05$, $n = 8$). The scale bars represent 100 μm in A.

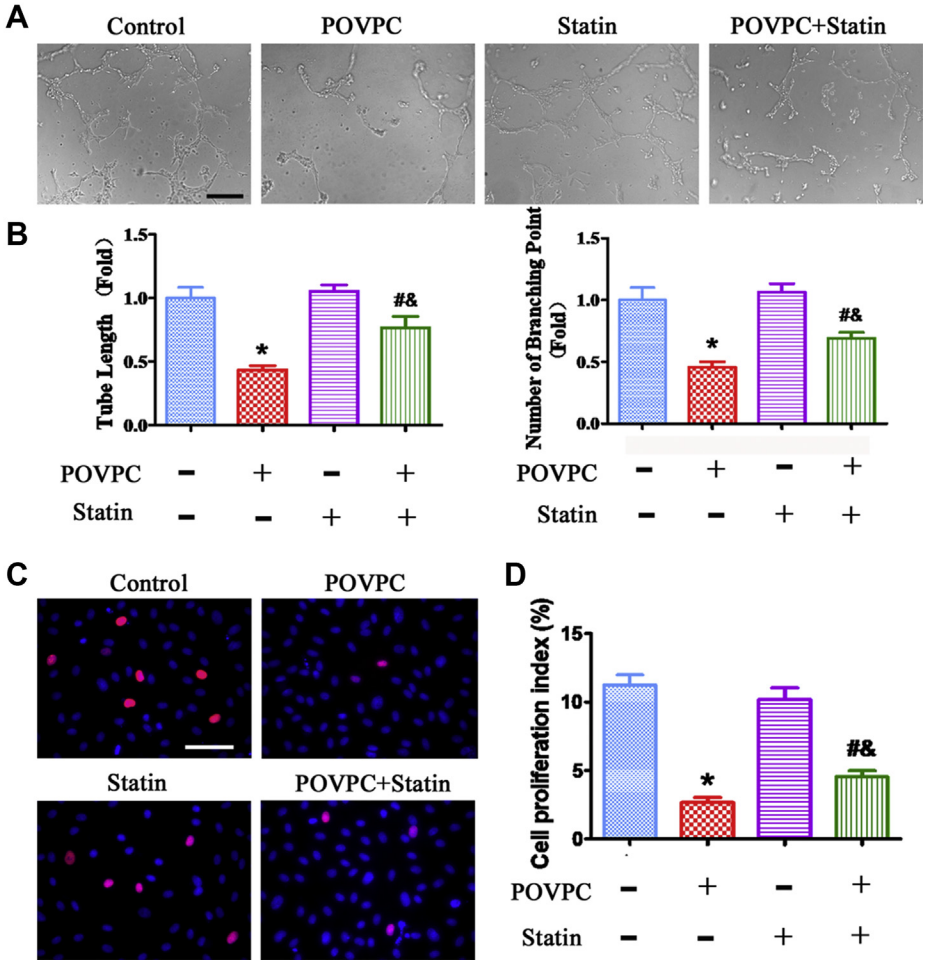

Fig. 3. Effects of POVPC and simvastatin on EC tube formation and proliferation. A: EC tube formation was photographed using a microscope after pretreatment with POVPC and simvastatin. B: Quantitative analysis of EC tube formation. C: EdU assay showing EC proliferation after pretreatment with POVPC and simvastatin. D: Analysis of percentages of EdU-positive cells (* vs. corresponding control group; # vs. POVPC group; & vs. statin group; $P < 0.05$, $n = 8$). The scale bars represent 200 μm in A and 100 μm in C.

generation were determined using DHE staining. DHE staining revealed that $O_2^{\bullet-}$ generation in ECs was significantly increased after POVPC pretreatment compared with basal conditions (**Fig. 4**A, B). The amount of $O_2^{\bullet-}$ in ECs treated with TNF-α served as a positive control. Manganese-5, 10, 15, 20-tetrakis (4-benzoic acid) porphyrin and L-NAME markedly inhibited $O_2^{\bullet-}$ generation, indicating that $O_2^{\bullet-}$ is generated from eNOS. Importantly, simvastatin significantly reduced POVPC-stimulated $O_2^{\bullet-}$ production (Fig. 4A, B).

Next, antioxidizing agent NAC, NADPH oxidase inhibitor DPI, and a mitochondrial complex I inhibitor, rotenone, were used to pretreat HUVECs, and then $O_2^{\bullet-}$ generation was detected after POVPC-induced EndMT. DHE staining showed that NAC completely inhibited $O_2^{\bullet-}$ generation, whereas DPI and rotenone partly blocked $O_2^{\bullet-}$ generation (Fig. 4C, D). Western blotting results showed that NAC, DPI, and rotenone clearly reversed the decrease in CD31 expression and attenuated the increase in α-SMA expression (Fig. 4E–H).

Effects of POVPC and simvastatin on NO generation in ECs

The effects of POVPC on NO generation in ECs were also examined. 4,5-Diaminofluoresce staining revealed that NO generation in ECs was significantly increased after VEGF stimulation compared with basal conditions (**Fig. 5**A, B). NO production was decreased in the POVPC treatment group. However, simvastatin significantly restored NO generation inhibited by POVPC (Fig. 5C). N^G-monomethyl-L-arginine inhibited NO production in all the groups (Fig. 5A, B).

Effects of POVPC and simvastatin on eNOS expression

The effects of POVPC and simvastatin on eNOS expression in ECs were then determined. POVPC decreased the expression of *eNOS* mRNAs, with a time-dependent manner (Fig. 5D). POVPC significantly reduced the expression of eNOS compared with the control in cultured HUVECs (Fig. 5E–H). As expected,

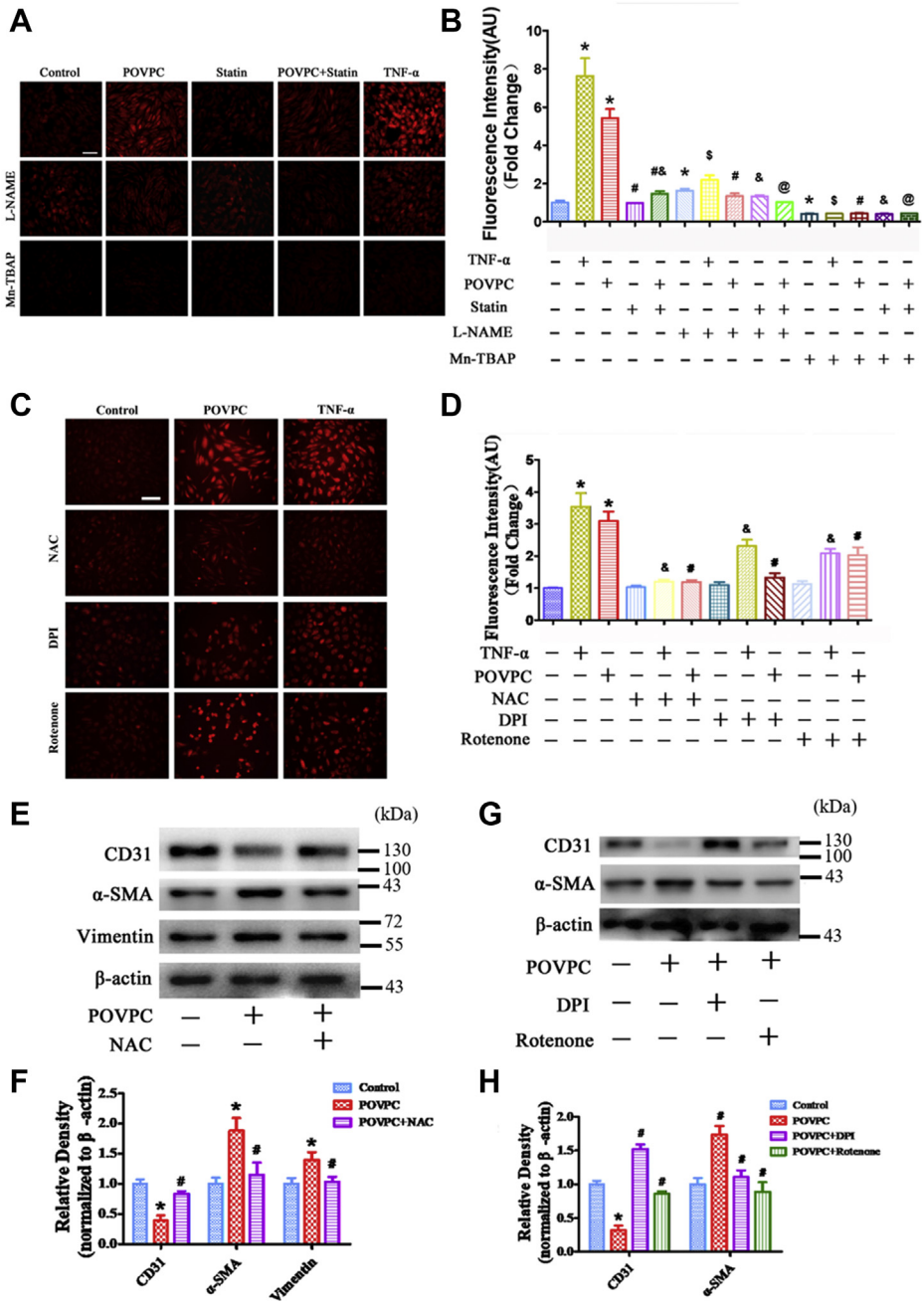

Fig. 4. Effects of POVPC and simvastatin on superoxide anion ($O_2^{\bullet-}$) production in cultured HUVECs. A and B: Intracellular levels of $O_2^{\bullet-}$ were detected using DHE after pretreatment of cultured HUVECs with POVPC with or without simvastatin. Only a small amount of $O_2^{\bullet-}$ was found in the control group (TNF-α treatment served as a positive control). POVPC treatment significantly increased $O_2^{\bullet-}$ generation. Mn-TBAP blocked the $O_2^{\bullet-}$ generation in both the TNF-α and POVPC groups. Simvastatin partly reduced $O_2^{\bullet-}$ generation induced by POVPC. L-NAME significantly reduced $O_2^{\bullet-}$ generation induced by POVPC and partially inhibited $O_2^{\bullet-}$ generation stimulated by TNF-α. C and D: Intracellular levels of $O_2^{\bullet-}$ was detected by DHE after pretreatment with NAC, DPI, and rotenone in cultured HUVECs. E and F: The Western blots and bar chart show the levels of CD31, α-SMA, and vimentin expression after NAC pretreated HUVECs. G and H: The Western blots and bar chart show the levels of CD31 and α-SMA expression after pretreated with DPI and rotenone in cultured HUVECs. (*vs. control group; #vs. POVPC group; &vs. statin group; $vs. TNF-α group; @vs. POVPC + statin group; $P < 0.05$, $n = 8$). The scale bars represent 100 μm in A and C.

simvastatin inhibited POVPC-mediated reduction in eNOS expression (Fig. 5E–H).

Effects of POVPC and simvastatin on TGF-β/Smad pathway

TGF-β is an effective fibrotic cytokine, and the Smad signaling pathway plays an important role in TGF-β-mediated fibrosis. Therefore, the effects of POVPC on the TGF-β/Smad signaling pathway were examined. POVPC significantly increased Smad2/3 expression, whereas simvastatin partly reversed the expression of Smad2/3 (**Fig. 6**A). In POVPC-treated HUVECs, the levels of phosphorylated Smad3, TGF-β, and TGF-β receptor II expression were increased

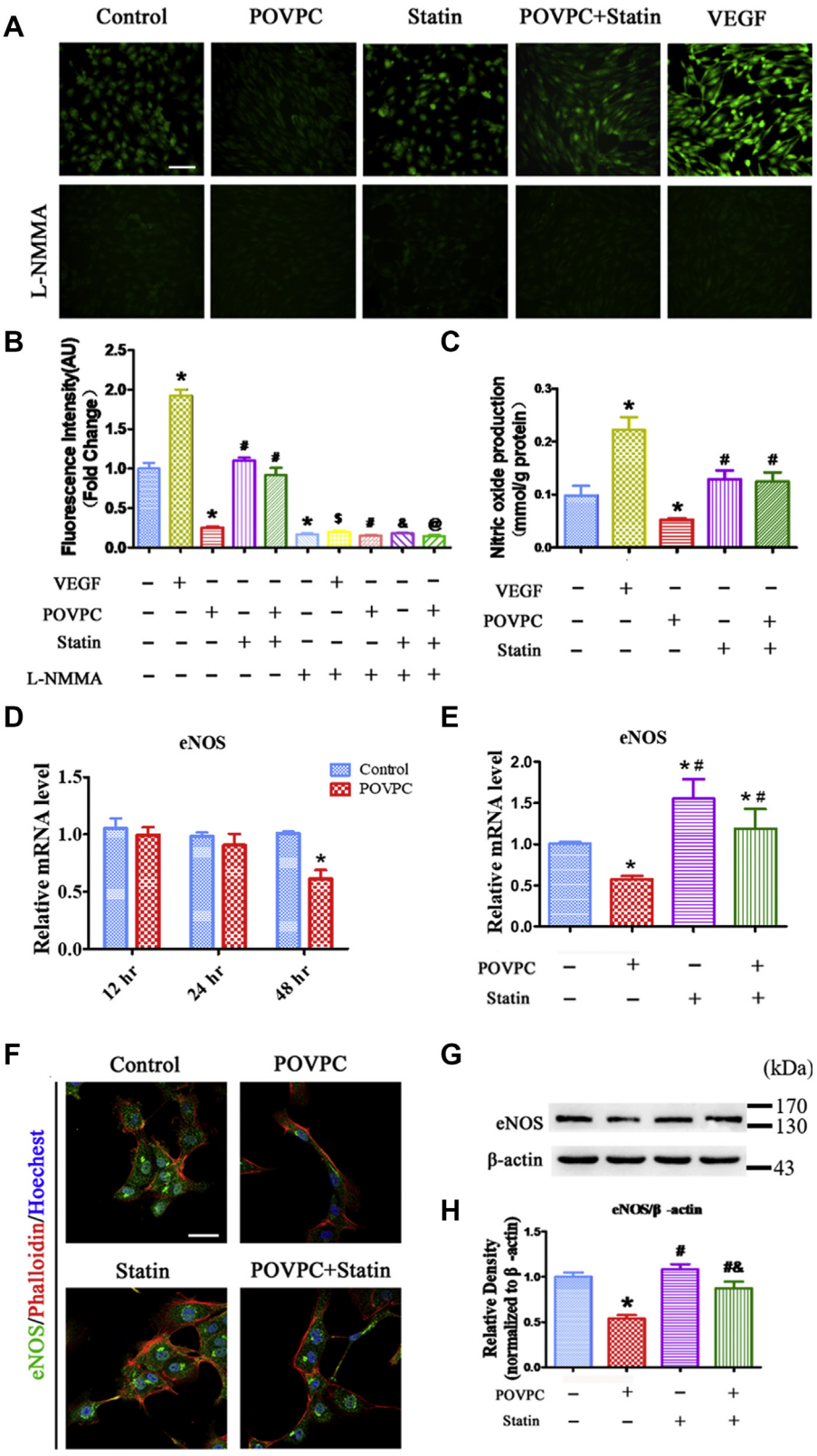

Fig. 5. Effects of POVPC and simvastatin on NO production and eNOS expression in cultured HUVECs. A and B: Intracellular levels of NO were detected by DAF-2DA fluorescence after pretreatment of cultured HUVECs with POVPC with or without simvastatin. Some NO staining is visible in the control group. VEGF significantly increased NO production. POVPC reduced NO production. Simvastatin did not affect NO production but inhibited POVPC-reduced NO production. L-NMMA treatment blocked NO production in all groups. C: Bar chart showing that POVPC markedly inhibited NO production in HUVECs using Sievers NOA analyzer methods. D: qRT-PCR showing the intracellular mRNA levels of *eNOS* after pretreated with POVPC for 12, 24, and 48 h in cultured HUVECs. E: qRT-PCR showing the intracellular mRNA levels of *eNOS* after pretreated with POVPC and/or simvastatin for 48 h in cultured HUVECs. F: HUVECs were analyzed by immunofluorescence for the expression of eNOS (green) after

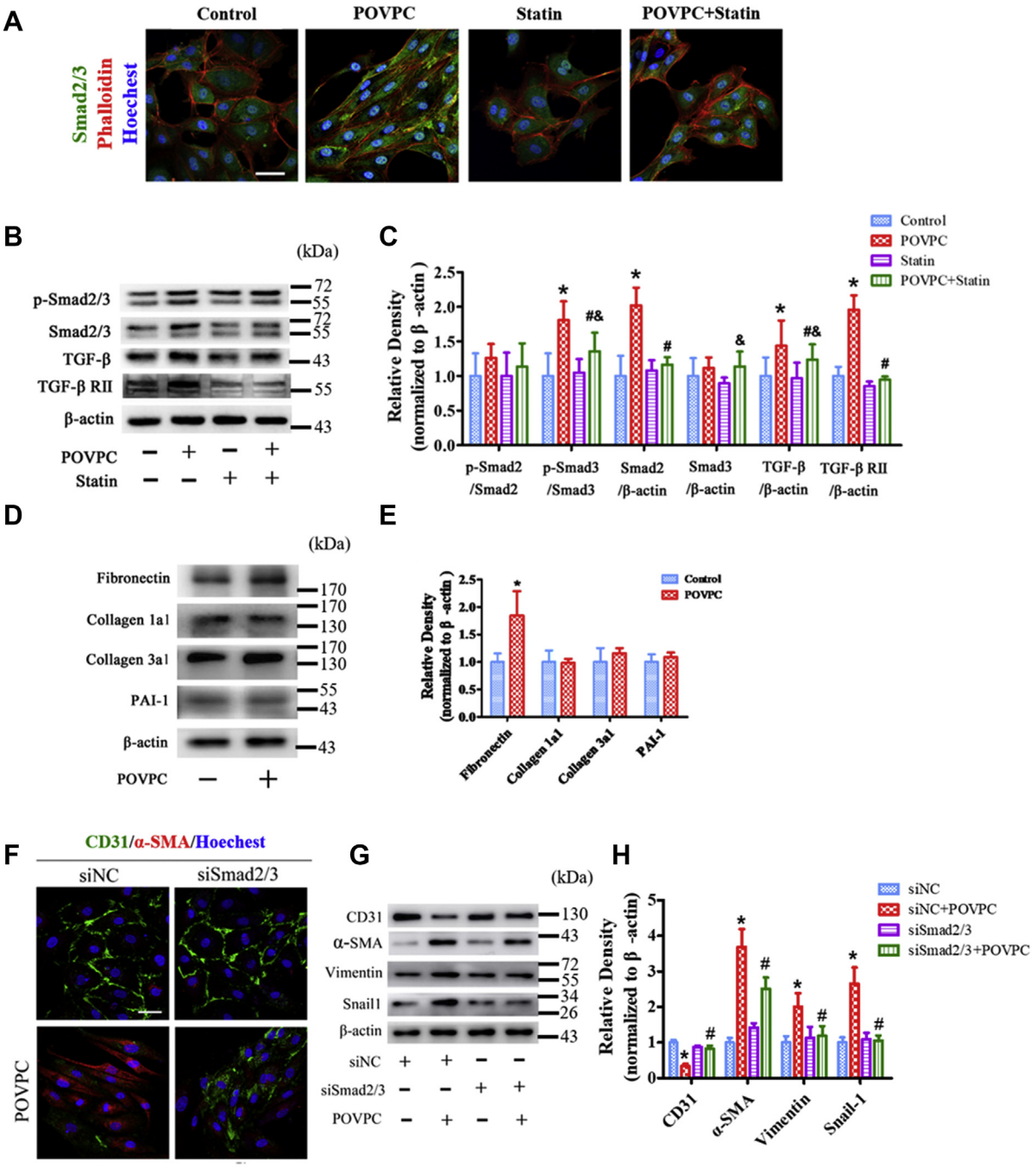

Fig. 6. Effects of POVPC and simvastatin on the TGF-β/Smad pathway in cultured HUVECs. A: HUVECs were analyzed by immunofluorescence for the expression of Smad2/3 (green) after pretreatment with POVPC with or without simvastatin. F-actin was stained with phalloidin (red). The nuclei were stained with Hoechst 33342 (blue). B and C: Western blots and bar charts showing the levels of p-Smad2, p-Smad3, Smad2, Smad3, TGF-β, and TGF-β receptor II (TGF-βRII) after pretreatment of cultured HUVECs with POVPC with or without simvastatin. D and E: The relative protein levels of fibronectin, collagen 1a1, collagen3a1, and plasminogen-activated inhibitor-1 (PAI-1) were assessed by Western blots in cultured HUVECs. F: Immunofluorescence analyzed the expression of CD31 and α-SMA in HUVECs after knockdown of *SMAD2/3* (siSmad2/3). G and H: The Wwestern blots and bar chart show the levels of CD31, α-SMA, vimentin and Snail-1 expression after knockdown *SMAD2/3* (siSmad2/3) (* versus control group; #vs. POVPC group; &vs. statin group; $P < 0.05$; $n = 8$). Scale bars represent 50 μm in A and F.

pretreatment with POVPC with or without simvastatin. F-actin was stained with phalloidin (red). The nuclei were stained with Hoechst 33342 (blue). G and H: Western blots and bar charts showing eNOS levels after pretreatment of the cultured HUVECs with POVPC with or without simvastatin (*vs. control group; #vs. POVPC group; &vs. statin group; $vs. VEGF group; @vs. POVPC + statin group; $P < 0.05$, $n = 8$). The scale bars represent 100 μm in A and 50 μm in F.

compared with that in the untreated cells. Simvastatin inhibited POVPC-induced increase in their protein expression (Fig. 6B, C). The marker genes downstream of TGF-β were also analyzed. POVPC only increased the expression of fibronectin, whereas the expression of collagen la1, collagen 3a1, and plasminogen-activated inhibitor-1 was not significantly different (Fig. 6D, E).

Next, we tested whether POVPC induced EndMT via Smad2/3. *SMAD2*-siRNA1–3 were selected to silence *SMAD2*, and *SMAD3*-siRNA2–3 were selected to silence *SMAD3*, respectively, as they demonstrated the maximum silencing effect (supplemental Fig. S3). Silencing of *SMAD2/3* markedly removed the POVPC-mediated suppression of CD31 expression and increased CD31 expression. In contrast, silencing of *SMAD2/3* markedly inhibited the expression of α-SMA, vimentin, and Snail-1 after POVPC-induced EndMT (Fig. 6F–H).

Effects of POVPC and simvastatin on Snail-1 and Twist-1 expression

Snail-1 and Twist-1 are known to promote epithelial to mesenchymal in cells. To further investigate the mechanisms by which POVPC induced EndMT via transcription factors, the effects of POVPC on Snail-1 and Twist-1 expression were examined. **Figure 7**A–C shows that the expression of Snail-1 and Twist-1 was significantly increased after POVPC treatment. In contrast, simvastatin inhibited POVPC-increased Snail-1 and Twist-1 expression.

Next, we determined whether POVPC induced EndMT via Snail-1 and Twist-1. *TWIST-1*-siRNA1–3 and *SNAIL-1*-siRNA were selected to silence *TWIST-1* and *SNAIL-1*. The silencing effect was showed in supplemental Fig. S4. Silencing of *SNAIL-1* and *TWIST-1* removed the suppression of POVPC on CD31 expression and markedly increased CD31 expression and inhibited the expression of α-SMA following POVPC-induced EndMT (Fig. 7D–H).

DISCUSSION

Plaque formation is a major pathological feature of atherosclerosis. Previous studies found that endothelial dysfunction, lipid retention, oxidative stress, and vascular fibrosis play important roles in the different stages of atherosclerotic plaque formation (35, 36). Plaque mainly comprises smooth muscle-like cells that may arise through migration and proliferation of smooth muscle cells from the media. However, recent studies suggest that smooth muscle-like cells are also derived from ECs through EndMT (9, 10, 37). EndMT may facilitate the acquisition of mesenchymal fate by ECs. Recent studies have demonstrated that EndMT plays a pivotal role in the pathogenesis of CVDs and may represent a novel therapeutic target for cardiovascular disorders. ECs become transformed into fibroblasts involved in vascular fibrotic remodeling

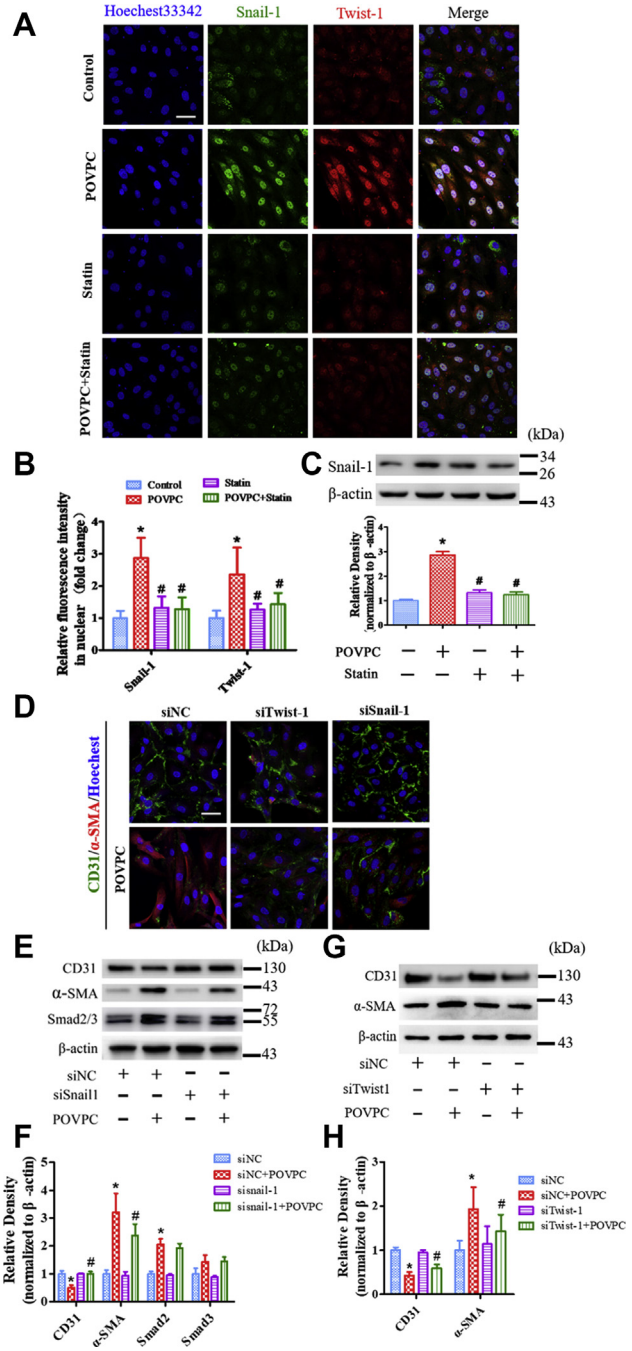

Fig. 7. Effects of POVPC and simvastatin on Snail-1 and Twist-1 expression in cultured HUVECs. A: HUVECs were analyzed by immunofluorescence for the expression of Snail-1 and Twist-1 after pretreatment with POVPC with or without simvastatin. B: Snail-1 nuclear localization was quantified by relative fluorescence intensity. C: The Western blots and bar charts showing the level of Snail-1 expression after pretreatment of cultured HUVECs with POVPC with or without simvastatin. D: Immunofluorescence analyzed the expression of CD31 and α-SMA in HUVECs after knockdown of *SNAIL-1* and *TWIST-1* (siSnail-1 and siTwist-1). E and F: The Western blots and bar chart show the levels of CD31, α-SMA, and Smad2/3 expression after knockdown of *SNAIL-1* (siSnail-1). G and H: The Western blots and bar chart show the levels of CD31 and α-SMA expression after knockdown of *TWIST-1* (siTwist-1) (*vs. control group; #vs. POVPC group; $P < 0.05$, $n = 8$). The scale bars represent 50 μm in A and D.

through EndMT during the pathological processes of atherosclerosis (9, 10, 37). Thus, EndMT plays a critical role in the development of atherosclerosis and plaque instability (10, 38).

EndMT can be induced by different stimulators or factors, including oxLDL (26, 27), hypercholesterolemia, hypoxia (39), inflammation (40), and oxidative stress (41, 42). oxLDL is a major lipoprotein deposited in atherosclerotic plaques, which is composed of many different lipid species. Proinflammatory factors, including oxLDL subfractions, have been found in atherosclerotic plaques and play an important role in different stages of the development of atherosclerosis (22, 43–45). POVPC, an oxidized phospholipid produced by oxidized PAPC, is found in atherosclerotic plaques and associated with chronic inflammation and vascular proliferation (46, 47). POVPC is a major component of minimally modified LDL and affects EC function (17, 20, 47). In the present study, we found that POVPC induced EndMT and impaired EC function, suggesting that oxLDL induces EndMT to promote atherosclerosis, at least in part, via POVPC. These data also support recent findings that oxidized phospholipids in oxLDL are proinflammatory and proatherogenic (14).

Oxidative stress is an important factor in the induction of EndMT (10, 48). Increased $O_2^{\bullet-}$ production enhances oxidative stress (49, 50). We recently showed that POVPC uncouples eNOS activity to produce $O_2^{\bullet-}$ instead of NO in ECs (23). Here, we also found that POVPC decreased NO production but increased $O_2^{\bullet-}$ generation in cultured ECs that was partially inhibited by L-NAME, indicating that one of the sources of POVPC-induced $O_2^{\bullet-}$ was from eNOS. In the control situation, L-NAME treatment increased $O_2^{\bullet-}$ generation in ECs as L-NAME is an NO synthase (NOS) inhibitor and inhibits NOS, resulting in the reduction of NO production, as described previously (23, 28, 32, 51–53). Without NO interaction with $O_2^{\bullet-}$ to form peroxynitrite in ECs, $O_2^{\bullet-}$ is released, which leads to an increase in $O_2^{\bullet-}$. However, when eNOS is uncoupled, L-NAME inhibits eNOS to generate $O_2^{\bullet-}$. As a result, $O_2^{\bullet-}$ generation decreases. Therefore, L-NAME inhibited POVPC-induced $O_2^{\bullet-}$ generation in ECs, suggesting that POVPC uncoupled eNOS activity.

Furthermore, we found that NAC, an antioxidizing agent, almost completely inhibited POVPC-induced $O_2^{\bullet-}$ generation, and DPI, an NADPH oxidase inhibitor, and rotenone, a mitochondrial complex I inhibitor, partially inhibited POVPC-induced $O_2^{\bullet-}$ generation. In addition, we found that POVPC partially suppressed eNOS phosphorylation. These findings suggest that the sources of reactive oxygen species induced by POVPC in the EndMT cells are from eNOS, NADPH oxidase, and mitochondria, respectively, and superoxide may be a potential mechanism underlying POVPC-induced EndMT. Consistent with this, EndMT is also promoted by the inhibition of NOS that reduces the bioavailability of NO and enhances oxidative stress (54). These data are consistent with our previous findings that POVPC uncouples NOS activity to produce $O_2^{\bullet-}$, which may increase oxidative stress resulting in EndMT. Bochkov *et al.* (55) demonstrated that POVPC stimulates VEGF expression, which may contribute to increased angiogenesis in advanced lesions and result in progression and destabilization of atherosclerotic plaques. They found that POVPC-stimulated VEGF expression was independent of hydroperoxide and free radicals. In their study, 84 μM of POVPC was used, which is higher than the 25 μM POVPC that was used in the present study. Gharavi *et al.* (47) also reported that L-NAME inhibits oxidized phospholipid-induced $O_2^{\bullet-}$ production from eNOS. In their study, oxidized PAPC and POVPC stimulated eNOS activity but induced $O_2^{\bullet-}$ production. These findings demonstrated that oxidized PAPC and POVPC uncouple eNOS activity, which is consistent with our findings. The concentration of POVPC used by them was also higher than the concentration used by us in the present study, suggesting that POVPC affects endothelial function via different mechanisms depending on its concentration.

Excessive activation of oxidative stress and overproduction of oxygen free radicals such as $O_2^{\bullet-}$ are known to promote the activation of TGF-β/Smad pathway injury in vascular ECs (56). TGF-β is considered a master regulator of EndMT and a key mediator of fibrosis that induces fibrotic diseases by activating downstream Smad signaling, termed "canonical TGF-β signaling" (9, 10). TGF-β is also the most potent chemotactic cytokine, and TGF-β expression is induced in most fibrotic diseases (57–59). Previous studies found that the Smad signaling pathway plays an important role in TGF-β-mediated fibrosis (42, 58). Therefore, TGF-β/Smad signaling is a critical factor in the maintenance of endothelial homeostasis. In the present study, we found that POVPC significantly upregulated the expression of TGF-β and activated Smad2/3 in vascular ECs, suggesting that POVPC promotes EndMT and fibrotic remodeling via the TGF-β/Smad signaling pathway.

TGF-β ligands also regulate EndMT by promoting the expression of the transcription factors Snail, Slug, and Twist (60). Snail-1, Slug, and Twist-1 repress the expression of endothelial marker genes, such as VE-cadherin and CD31, and facilitate the expression of mesenchymal genes to regulate EndMT (61, 62). Snail-1 is present in luminal ECs overlying human coronary artery plaques, and Snail-1 and Twist-1 are expressed in luminal ECs in the atheroprone areas of the aorta (63, 64). Gata-4 regulates Twist-1 expression, which in turn induces Snail-1 in ECs (64). However, the upstream regulators and downstream targets of this pathway remain unclear and may include TGF-β, Notch, and Wnt signaling (61, 65, 66). In addition, oxLDL induces EndMT by stabilizing Snail in human ECs (26). In the present study, Twist-1 and Snail-1 were highly activated by POVPC, indicating that POVPC may induce oxidative stress to stimulate the canonical TGF-β/Smad

signaling pathway, resulting in the activation of Twist-1 and Snail-1 that causes EndMT.

Statins have been used to prevent or treat atherosclerosis for several decades. Statins are lipid-lowering drugs that especially reduce LDL levels (24, 25). Statins significantly prevent endothelial dysfunction by reducing oxidative stress (67), and attenuate renal injury through the TGF-β/Smad signaling pathway, and by suppressing oxidative stress (68). Simvastatin is a statin that inhibits oxLDL-induced proatherogenic effects (24). Therefore, we investigated whether simvastatin inhibits POVPC-induced EndMT. We found that simvastatin partly attenuates POVPC-induced EndMT in ECs, which occurred through suppression of the TGF-β/Smad/Snail signaling pathway. These data suggest that simvastatin may inhibit atherosclerosis, at least in part, through the reduction of POVPC-induced EndMT. Therefore, another primary novel finding in our study was that simvastatin protected HUVECs from POVPC-induced EndMT via suppression of oxidative stress.

In summary, our findings demonstrated that POVPC induces oxidative stress to promote the expression of TGF-β/Smad, leading to the activation of Twist-1 and Snail-1 that causes EC dysfunction and mediates the occurrence of EndMT. These effects may promote fibrotic remodeling and accelerate the process of atherosclerosis. Simvastatin may inhibit atherosclerosis by preventing POVPC-induced oxidative stress, the activation of TGF-β/Smad, Twist-1, and Snail-1, EC dysfunction, and EndMT. Our findings reveal novel mechanisms by which POVPC promotes the development of atherosclerosis, and simvastatin inhibits atherosclerosis. Our findings also suggest that POVPC may be a potential therapeutic target for inhibition of atherosclerosis.

Data availability

All data are contained within the article.

Supplemental data

This article contains supplemental data.

Acknowledgments

The authors thank the staffs at the First Affiliated Hospital, Sun Yat-sen University for their assistance throughout this study. This research was financially supported by the National Natural Science Foundation of China (grants 81970363, 81830013, 81370370, 81670392, 81600382, 81770241, and Distinguished Young Scholar grant 81325001), Guangdong Natural Science Fund Committee (grant 2015A030312009), Guangdong Basic and Applied Basic Research Foundation (grant 2019B1515120092), International Cooperation Project (2015DFA31070), and National Key R&D Program (2016YFC0903000) from the Ministry of Science and Technology of the People's Republic of China, the Changjiang Scholars Program from the Ministry of Education of China, the Guangdong Pearl River Scholars Program, and the Sun Yat-sen University Clinical Research 5010 Program. The five and five projects are from The First Affiliated Hospital, Sun Yat-sen University and Program of National Key Clinical Specialties, Fundamental Research Funds for the Central Universities Sun Yat-sen University Young Teacher Training Program (19ykpy79).

Author contributions

J.- S. O. and Z.- J. O. conception and design of research. Y. L., Y.- X. Z., D.- S. N., J. C., S.- X. L., Z.- W. M., Y.- M. P. performed the experiments. Y. L., Y.- X. Z., D.- S. N., J. C., S.- X. L., S.- H. H., Y.- T. C., C.- J. Z., and H.- X. Y. analyzed the data. Y. L., Y.- X. Z., D.- S. N., J. C., S.- X. L., Z.- W. M., Y.- M. P., J.- J. G., J.- S. O., and Z.- J. O. interpreted the results of experiments. Y. L., Y.- X. Z., D.- S. N., S.- X. L. and H.- X. Y. prepared the figures. Y. L., Y.- X. Z., D.- S. N., J. C., S.- X. L., J.- S. O., and Z.- J. O. drafted the article. J.- S. O. and Z.- J. O. edited and revised the article as well as approved the final version of the article.

Conflict of interest

The authors declare that they have no conflicts of interest with the contents of this article.

Abbreviations

CCK-8, Cell Counting Kit-8; DHE, dihydroethidium; DPI, diphenyleneiodonium; EC, endothelial cell; EdU, 5-ethynyl-20-deoxyuridine; EndMT, endothelial-to-mesenchymal transition; HUVECs, human umbilical vein endothelial cells; L-NAME, N(ω)-nitro-L-arginine methyl ester; NAC, *N*-acetylcysteine; NOS, NO synthase; oxLDL, oxidized LDL; PAPC, 1-palmitoyl-2-arachidonoyl-sn-glycero-3-phosphatidylcholine; POVPC, 1-palmitoyl-2-(5-oxovaleroyl)-sn-glycero-3-phosphocholine; qRT, quantitative RT; α-SMA, alpha-smooth muscle actin; TGF-β, transforming growth factor-beta; VE, vascular endothelial; VEGF, vascular endothelial growth factor.

Manuscript received July 31, 2020, and in revised from February 22, 2021. Published, JLR Papers in Press, March 10, 2021, https://doi.org/10.1016/j.jlr.2021.100066

REFERENCES

1. Nguyen, M. T., Fernando, S., Schwarz, N., Tan, J. T., Bursill, C. A., and Psaltis, P. J. (2019) Inflammation as a therapeutic target in atherosclerosis. *J. Clin. Med.* **8**, 1109
2. Nazarian-Samani, Z., Sewell, R. D. E., and Rafieian-Kopaei, M. (2020) Inflammasome signaling and other factors implicated in atherosclerosis development and progression. *Curr. Pharm. Des.* **26**, 2583–2590
3. Gimbrone, M. A., Jr., and Garcia-Cardena, G. (2016) Endothelial cell dysfunction and the pathobiology of atherosclerosis. *Circ. Res.* **118**, 620–636
4. Piera-Velazquez, S., Mendoza, F. A., and Jimenez, S. A. (2016) Endothelial to mesenchymal transition (EndoMT) in the pathogenesis of human fibrotic diseases. *J. Clin. Med.* **5**, 45
5. Ranchoux, B., Antigny, F., Rucker-Martin, C., Hautefort, A., Pechoux, C., Bogaard, H. J., Dorfmuller, P., Remy, S., Lecerf, F., Plante, S., Chat, S., Fadel, E., Houssaini, A., Anegon, I., Adnot, S., *et al.* (2015) Endothelial-to-mesenchymal transition in pulmonary hypertension. *Circulation.* **131**, 1006–1018
6. Souilhol, C., Harmsen, M. C., Evans, P. C., and Krenning, G. (2018) Endothelial-mesenchymal transition in atherosclerosis. *Cardiovasc. Res.* **114**, 565–577
7. Calandrelli, R., Xu, L. X., Luo, Y. J., Wu, W. X., Fan, X. C., Nguyen, T., Chen, C. J., Sriram, K., Tang, X. F., Burns, A. B., Natarajan, R., Chen, Z. B. M., and Zhong, S. (2020) Stress-induced

RNA-chromatin interactions promote endothelial dysfunction. *Nat. Commun.* **11**, 5211
8. He, M., Chen, Z., Martin, M., Zhang, J., Sangwung, P., Woo, B., Tremoulet, A. H., Shimizu, C., Jain, M. K., Burns, J. C., and Shyy, J. Y. (2017) miR-483 targeting of CTGF suppresses endothelial-to-mesenchymal transition: therapeutic implications in kawasaki disease. *Circ. Res.* **120**, 354–365
9. Chen, P. Y., Qin, L., Baeyens, N., Li, G., Afolabi, T., Budatha, M., Tellides, G., Schwartz, M. A., and Simons, M. (2015) Endothelial-to-mesenchymal transition drives atherosclerosis progression. *J. Clin. Invest.* **125**, 4514–4528
10. Evrard, S. M., Lecce, L., Michelis, K. C., Nomura-Kitabayashi, A., Pandey, G., Purushothaman, K. R., d'Escamard, V., Li, J. R., Hadri, L., Fujitani, K., Moreno, P. R., Benard, L., Rimmele, P., Cohain, A., Mecham, B., *et al.* (2016) Endothelial to mesenchymal transition is common in atherosclerotic lesions and is associated with plaque instability. *Nat. Commun.* **7**, 11853
11. Maleszewska, M., Moonen, J. R., Huijkman, N., van de Sluis, B., Krenning, G., and Harmsen, M. C. (2013) IL-1beta and TGFbeta2 synergistically induce endothelial to mesenchymal transition in an NFkappaB-dependent manner. *Immunobiology.* **218**, 443–454
12. Kovacic, J. C., Dimmeler, S., Harvey, R. P., Finkel, T., Aikawa, E., Krenning, G., and Baker, A. H. (2019) Endothelial to mesenchymal transition in cardiovascular disease: JACC state-of-the-art review. *J. Am. Coll. Cardiol.* **73**, 190–209
13. Pidkovka, N. A., Cherepanova, O. A., Yoshida, T., Alexander, M. R., Deaton, R. A., Thomas, J. A., Leitinger, N., and Owens, G. K. (2007) Oxidized phospholipids induce phenotypic switching of vascular smooth muscle cells in vivo and in vitro. *Circ. Res.* **101**, 792–801
14. Que, X., Hung, M. Y., Yeang, C., Gonen, A., Prohaska, T. A., Sun, X., Diehl, C., Maatta, A., Gaddis, D. E., Bowden, K., Pattison, J., MacDonald, J. G., Yla-Herttuala, S., Mellon, P. L., Hedrick, C. C., *et al.* (2018) Oxidized phospholipids are proinflammatory and proatherogenic in hypercholesterolaemic mice. *Nature.* **558**, 301–306
15. Ayee, M. A., LeMaster, E., Shentu, T. P., Singh, D. K., Barbera, N., Soni, D., Tiruppathi, C., Subbaiah, P. V., Berdyshev, E., Bronova, I., Cho, M., Akpa, B. S., and Levitan, I. (2017) Molecular-scale biophysical modulation of an endothelial membrane by oxidized phospholipids. *Biophys. J.* **112**, 325–338
16. Pegorier, S., Stengel, D., Durand, H., Croset, M., and Ninio, E. (2006) Oxidized phospholipid: POVPC binds to platelet-activating-factor receptor on human macrophages. Implications in atherosclerosis. *Atherosclerosis.* **188**, 433–443
17. Watson, A. D., Leitinger, N., Navab, M., Faull, K. F., Horkko, S., Witztum, J. L., Palinski, W., Schwenke, D., Salomon, R. G., Sha, W., Subbanagounder, G., Fogelman, A. M., and Berliner, J. A. (1997) Structural identification by mass spectrometry of oxidized phospholipids in minimally oxidized low density lipoprotein that induce monocyte/endothelial interactions and evidence for their presence in vivo. *J. Biol. Chem.* **272**, 13597–13607
18. Subbanagounder, G., Leitinger, N., Schwenke, D. C., Wong, J. W., Lee, H., Rizza, C., Watson, A. D., Faull, K. F., Fogelman, A. M., and Berliner, J. A. (2000) Determinants of bioactivity of oxidized phospholipids. Specific oxidized fatty acyl groups at the sn-2 position. *Arterioscler. Thromb. Vasc. Biol.* **20**, 2248–2254
19. Cherepanova, O. A., Pidkovka, N. A., Sarmento, O. F., Yoshida, T., Gan, Q., Adiguzel, E., Bendeck, M. P., Berliner, J., Leitinger, N., and Owens, G. K. (2009) Oxidized phospholipids induce type VIII collagen expression and vascular smooth muscle cell migration. *Circ. Res.* **104**, 609–618
20. Yeh, M., Cole, A. L., Choi, J., Liu, Y., Tulchinsky, D., Qiao, J. H., Fishbein, M. C., Dooley, A. N., Hovnanian, T., Mouilleseaux, K., Vora, D. K., Yang, W. P., Gargalovic, P., Kirchgessner, T., Shyy, J. Y., *et al.* (2004) Role for sterol regulatory element-binding protein in activation of endothelial cells by phospholipid oxidation products. *Circ. Res.* **95**, 780–788
21. Afonyushkin, T., Oskolkova, O. V., Philippova, M., Resink, T. J., Erne, P., Binder, B. R., and Bochkov, V. N. (2010) Oxidized phospholipids regulate expression of ATF4 and VEGF in endothelial cells via NRF2-dependent mechanism: novel point of convergence between electrophilic and unfolded protein stress pathways. *Arterioscler. Thromb. Vasc. Biol.* **30**, 1007–1013
22. Yeh, M., Leitinger, N., de Martin, R., Onai, N., Matsushima, K., Vora, D. K., Berliner, J. A., and Reddy, S. T. (2001) Increased transcription of IL-8 in endothelial cells is differentially regulated by TNF-alpha and oxidized phospholipids. *Arterioscler. Thromb. Vasc. Biol.* **21**, 1585–1591
23. Yan, F. X., Li, H. M., Li, S. X., He, S. H., Dai, W. P., Li, Y., Wang, T. T., Shi, M. M., Yuan, H. X., Xu, Z., Zhou, J. G., Ning, D. S., Mo, Z. W., Ou, Z. J., and Ou, J. S. (2017) The oxidized phospholipid POVPC impairs endothelial function and vasodilation via uncoupling endothelial nitric oxide synthase. *J. Mol. Cell Cardiol.* **112**, 40–48
24. Yang, X., Yin, M., Yu, L., Lu, M., Wang, H., Tang, F., and Zhang, Y. (2016) Simvastatin inhibited oxLDL-induced proatherogenic effects through calpain-1-PPARgamma-CD36 pathway. *Can. J. Physiol. Pharmacol.* **94**, 1336–1343
25. Harisa, G. I., Alomrani, A. H., and Badran, M. M. (2017) Simvastatin-loaded nanostructured lipid carriers attenuate the atherogenic risk of erythrocytes in hyperlipidemic rats. *Eur. J. Pharm. Sci.* **96**, 62–71
26. Su, Q., Sun, Y., Ye, Z., Yang, H., and Li, L. (2018) Oxidized low density lipoprotein induces endothelial-to-mesenchymal transition by stabilizing Snail in human aortic endothelial cells. *Biomed. Pharmacother.* **106**, 1720–1726
27. Gong, L., Lei, Y., Liu, Y., Tan, F., Li, S., Wang, X., Xu, M., Cai, W., Du, B., Xu, F., Zhou, Y., Han, H., Sun, H., and Qiu, L. (2019) Vaccarin prevents ox-LDL-induced HUVEC EndMT, inflammation and apoptosis by suppressing ROS/p38 MAPK signaling. *Am. J. Transl. Res.* **11**, 2140–2154
28. Ou, Z. J., Chen, J., Dai, W. P., Liu, X., Yang, Y. K., Li, Y., Lin, Z. B., Wang, T. T., Wu, Y. Y., Su, D. H., Cheng, T. P., Wang, Z. P., Tao, J., and Ou, J. S. (2016) 25-Hydroxycholesterol impairs endothelial function and vasodilation by uncoupling and inhibiting endothelial nitric oxide synthase. *Am. J. Physiol. Endocrinol. Metab.* **311**, E781–E790
29. Ci, H. B., Ou, Z. J., Chang, F. J., Liu, D. H., He, G. W., Xu, Z., Yuan, H. Y., Wang, Z. P., Zhang, X., and Ou, J. S. (2013) Endothelial microparticles increase in mitral valve disease and impair mitral valve endothelial function. *Am. J. Physiol. Endocrinol. Metab.* **304**, E695–702
30. Fu, L., Hu, X. X., Lin, Z. B., Chang, F. J., Ou, Z. J., Wang, Z. P., and Ou, J. S. (2015) Circulating microparticles from patients with valvular heart disease and cardiac surgery inhibit endothelium-dependent vasodilation. *J. Thorac. Cardiovasc. Surg.* **150**, 666–672
31. Chang, F. J., Yuan, H. Y., Hu, X. X., Ou, Z. J., Fu, L., Lin, Z. B., Wang, Z. P., Wang, S. M., Zhou, L., Xu, Y. Q., Wang, C. P., Xu, Z., Zhang, X., Zhang, C. X., and Ou, J. S. (2014) High density lipoprotein from patients with valvular heart disease uncouples endothelial nitric oxide synthase. *J. Mol. Cell Cardiol.* **74**, 209–219
32. Ou, Z., Ou, J., Ackerman, A. W., Oldham, K. T., and Pritchard, K. A., Jr. (2003) L-4F, an apolipoprotein A-1 mimetic, restores nitric oxide and superoxide anion balance in low-density lipoprotein-treated endothelial cells. *Circulation.* **107**, 1520–1524
33. Li, H. M., Mo, Z. W., Peng, Y. M., Li, Y., Dai, W. P., Yuan, H. Y., Chang, F. J., Wang, T. T., Wang, M., Hu, K. H., Li, X. D., Ning, D. S., Chen, Y. T., Song, Y. K., Lu, X. L., *et al.* (2020) Angiogenic and Antiangiogenic mechanisms of high density lipoprotein from healthy subjects and coronary artery diseases patients. *Redox Biol.* **36**, 101642
34. Medici, D., Potenta, S., and Kalluri, R. (2011) Transforming growth factor-beta2 promotes Snail-mediated endothelial-mesenchymal transition through convergence of Smad-dependent and Smad-independent signalling. *Biochem. J.* **437**, 515–520
35. Khyzha, N., Alizada, A., Wilson, M. D., and Fish, J. E. (2017) Epigenetics of atherosclerosis: emerging mechanisms and methods. *Trends Mol. Med.* **23**, 332–347
36. Gistera, A., and Hansson, G. K. (2017) The immunology of atherosclerosis. *Nat. Rev. Nephrol.* **13**, 368–380
37. Moonen, J. R., Lee, E. S., Schmidt, M., Maleszewska, M., Koerts, J. A., Brouwer, L. A., van Kooten, T. G., van Luyn, M. J., Zeebregts, C. J., Krenning, G., and Harmsen, M. C. (2015) Endothelial-to-mesenchymal transition contributes to fibro-proliferative vascular disease and is modulated by fluid shear stress. *Cardiovasc. Res.* **108**, 377–386
38. Vanchin, B., Offringa, E., Friedrich, J., Brinker, M. G., Kiers, B., Pereira, A. C., Harmsen, M. C., Moonen, J. A., and Krenning, G. (2019) MicroRNA-374b induces endothelial-to-mesenchymal transition and early lesion formation through the inhibition of MAPK7 signaling. *J. Pathol.* **247**, 456–470
39. Doerr, M., Morrison, J., Bergeron, L., Coomber, B. L., and Viloria-Petit, A. (2016) Differential effect of hypoxia on early endothelial-mesenchymal transition response to transforming growth beta isoforms 1 and 2. *Microvasc. Res.* **108**, 48–63

40. Sanchez-Duffhues, G., Garcia de Vinuesa, A., van de Pol, V., Geerts, M. E., de Vries, M. R., Janson, S. G., van Dam, H., Lindeman, J. H., Goumans, M. J., and Ten Dijke, P. (2019) Inflammation induces endothelial-to-mesenchymal transition and promotes vascular calcification through downregulation of BMPR2. *J. Pathol.* **247**, 333–346
41. Thuan, D. T. B., Zayed, H., Eid, A. H., Abou-Saleh, H., Nasrallah, G. K., Mangoni, A. A., and Pintus, G. (2018) A potential link between oxidative stress and endothelial-to-mesenchymal transition in systemic sclerosis. *Front. Immunol.* **9**, 1985
42. Hiraga, R., Kato, M., Miyagawa, S., and Kamata, T. (2013) Nox4-derived ROS signaling contributes to TGF-beta-induced epithelial-mesenchymal transition in pancreatic cancer cells. *Anticancer Res.* **33**, 4431–4438
43. Ravandi, A., Leibundgut, G., Hung, M. Y., Patel, M., Hutchins, P. M., Murphy, R. C., Prasad, A., Mahmud, E., Miller, Y. I., Dennis, E. A., Witztum, J. L., and Tsimikas, S. (2014) Release and capture of bioactive oxidized phospholipids and oxidized cholesteryl esters during percutaneous coronary and peripheral arterial interventions in humans. *J. Am. Coll. Cardiol.* **63**, 1961–1971
44. Qin, X., and Guo, J. (2020) MicroRNA-328-3p protects vascular endothelial cells against oxidized low-density lipoprotein induced injury via targeting forkhead box protein O4 (FOXO4) in atherosclerosis. *Med. Sci. Monit.* **26**, e921877
45. Reis, A. (2017) Oxidative Phospholipidomics in health and disease: achievements, challenges and hopes. *Free Radic. Biol. Med.* **111**, 25–37
46. Fruhwirth, G. O., Moumtzi, A., Loidl, A., Ingolic, E., and Hermetter, A. (2006) The oxidized phospholipids POVPC and PGPC inhibit growth and induce apoptosis in vascular smooth muscle cells. *Biochim. Biophys. Acta.* **1761**, 1060–1069
47. Gharavi, N. M., Baker, N. A., Mouillesseaux, K. P., Yeung, W., Honda, H. M., Hsieh, X., Yeh, M., Smart, E. J., and Berliner, J. A. (2006) Role of endothelial nitric oxide synthase in the regulation of SREBP activation by oxidized phospholipids. *Circ. Res.* **98**, 768–776
48. Li, J., Zhang, Q., Ren, C., Wu, X., Zhang, Y., Bai, X., Lin, Y., Li, M., Fu, J., Kopylov, P., Wang, S., Yu, T., Wang, N., Xu, C., Zhang, Y., *et al.* (2018) Low-intensity pulsed ultrasound prevents the oxidative stress induced endothelial-mesenchymal transition in human aortic endothelial cells. *Cell Physiol. Biochem.* **45**, 1350–1365
49. Chang, J. P., Chen, M. C., Liu, W. H., Yang, C. H., Chen, C. J., Chen, Y. L., Pan, K. L., Tsai, T. H., and Chang, H. W. (2011) Atrial myocardial nox2 containing NADPH oxidase activity contribution to oxidative stress in mitral regurgitation: potential mechanism for atrial remodeling. *Cardiovasc. Pathol.* **20**, 99–106
50. Corradi, D., Callegari, S., Maestri, R., Benussi, S., Bosio, S., De Palma, G., Alinovi, R., Caglieri, A., Goldoni, M., Mozzoni, P., Pastori, P., Manotti, L., Nascimbene, S., Dorigo, E., Rusconi, R., *et al.* (2008) Heme oxygenase-1 expression in the left atrial myocardium of patients with chronic atrial fibrillation related to mitral valve disease: its regional relationship with structural remodeling. *Hum. Pathol.* **39**, 1162–1171
51. Ou, J., Ou, Z., Ackerman, A. W., Oldham, K. T., and Pritchard, K. A., Jr. (2003) Inhibition of heat shock protein 90 (hsp90) in proliferating endothelial cells uncouples endothelial nitric oxide synthase activity. *Free Radic. Biol. Med.* **34**, 269–276
52. Ou, J., Ou, Z., McCarver, D. G., Hines, R. N., Oldham, K. T., Ackerman, A. W., and Pritchard, K. A., Jr. (2003) Trichloroethylene decreases heat shock protein 90 interactions with endothelial nitric oxide synthase: implications for endothelial cell proliferation. *Toxicol. Sci.* **73**, 90–97
53. Ou, J., Fontana, J. T., Ou, Z., Jones, D. W., Ackerman, A. W., Oldham, K. T., Yu, J., Sessa, W. C., and Pritchard, K. A., Jr. (2004) Heat shock protein 90 and tyrosine kinase regulate eNOS NO* generation but not NO* bioactivity. *Am. J. Physiol. Heart Circ. Physiol.* **286**, H561–569
54. O'Riordan, E., Mendelev, N., Patschan, S., Patschan, D., Eskander, J., Cohen-Gould, L., Chander, P., and Goligorsky, M. S. (2007) Chronic NOS inhibition actuates endothelial-mesenchymal transformation. *Am. J. Physiol. Heart Circ. Physiol.* **292**, H285–294
55. Bochkov, V. N., Philippova, M., Oskolkova, O., Kadl, A., Furnkranz, A., Karabeg, E., Afonyushkin, T., Gruber, F., Breuss, J., Minchenko, A., Mechtcheriakova, D., Hohensinner, P., Rychli, K., Wojta, J., Resink, T., *et al.* (2006) Oxidized phospholipids stimulate angiogenesis via autocrine mechanisms, implicating a novel role for lipid oxidation in the evolution of atherosclerotic lesions. *Circ. Res.* **99**, 900–908
56. Wang, Y., Che, J., Zhao, H., Tang, J., and Shi, G. (2018) Osthole alleviates oxidized low-density lipoprotein-induced vascular endothelial injury through suppression of transforming growth factor-beta1/Smad pathway. *Int. Immunopharmacol.* **65**, 373–381
57. Pardali E, S-D. G., Gomez-Puerto, M. C., and Ten Dijke, P. (2017) TGF-β-induced endothelial-mesenchymal transition in fibrotic diseases. *Int. J. Mol. Sci.* **18**, 2157
58. Xu F, L. C., Zhou, D., and Zhang, L. (2016) TGF-β/SMAD pathway and its regulation in hepatic fibrosis. *J. Histochem. Cytochem.* **64**, 157–167
59. Y, I. (2018) Targeting TGF-β signaling in kidney fibrosis. *Int. J. Mol. Sci.* **19**, 2532
60. Hata, A., and Chen, Y. G. (2016) TGF-beta signaling from receptors to Smads. *Cold Spring Harb. Perspect. Biol.* **8**, a022061
61. Kokudo, T., Suzuki, Y., Yoshimatsu, Y., Yamazaki, T., Watabe, T., and Miyazono, K. (2008) Snail is required for TGFbeta-induced endothelial-mesenchymal transition of embryonic stem cell-derived endothelial cells. *J. Cell Sci.* **121**, 3317–3324
62. Lopez, D., Niu, G., Huber, P., and Carter, W. B. (2009) Tumor-induced upregulation of Twist, Snail, and Slug represses the activity of the human VE-cadherin promoter. *Arch. Biochem. Biophys.* **482**, 77–82
63. Mahmoud, M. M., Serbanovic-Canic, J., Feng, S., Souilhol, C., Xing, R., Hsiao, S., Mammoto, A., Chen, J., Ariaans, M., Francis, S. E., Van der Heiden, K., Ridger, V., and Evans, P. C. (2017) Shear stress induces endothelial-to-mesenchymal transition via the transcription factor Snail. *Sci. Rep.* **7**, 3375
64. Mahmoud, M. M., Kim, H. R., Xing, R., Hsiao, S., Mammoto, A., Chen, J., Serbanovic-Canic, J., Feng, S., Bowden, N. P., Maguire, R., Ariaans, M., Francis, S. E., Weinberg, P. D., van der Heiden, K., Jones, E. A., *et al.* (2016) TWIST1 integrates endothelial responses to flow in vascular dysfunction and atherosclerosis. *Circ. Res.* **119**, 450–462
65. Niessen, K., Fu, Y., Chang, L., Hoodless, P. A., McFadden, D., and Karsan, A. (2008) Slug is a direct Notch target required for initiation of cardiac cushion cellularization. *J. Cell Biol.* **182**, 315–325
66. Aisagbonhi, O., Rai, M., Ryzhov, S., Atria, N., Feoktistov, I., and Hatzopoulos, A. K. (2011) Experimental myocardial infarction triggers canonical Wnt signaling and endothelial-to-mesenchymal transition. *Dis. Model Mech.* **4**, 469–483
67. Wang, F., Ma, H., Liang, W. J., Yang, J. J., Wang, X. Q., Shan, M. R., Chen, Y., Jia, M., Yin, Y. L., Sun, X. Y., Zhang, J. N., Peng, Q. S., Chen, Y. G., Liu, L. Y., Li, P., *et al.* (2017) Lovastatin upregulates microRNA-29b to reduce oxidative stress in rats with multiple cardiovascular risk factors. *Oncotarget.* **8**, 9021–9034
68. Ma, Z., Zhu, L., Liu, Y., Wang, Z., Yang, Y., Chen, L., and Lu, Q. (2017) Lovastatin alleviates endothelial-to-mesenchymal transition in glomeruli via suppression of oxidative stress and TGF-beta1 signaling. *Front. Pharmacol.* **8**, 473